Monomeric α-Synuclein Binds Congo Red Micelles in a Disordered Manner

Alexander S. Maltsev, Alexander Grishaev, and Ad Bax*

Laboratory of Chemical Physics, National Institute of Diabetes and Digestive and Kidney Diseases, National Institutes of Health, Bethesda, Maryland 20892-0520, United States

ⓈSupporting Information

ABSTRACT: The histological dye Congo Red (CR) previously has been shown to inhibit α-synuclein (aS) fibrillation, but the mode of this inhibition remained unclear. Because of favorable exchange kinetics, interaction between CR and aS lends itself to a detailed nuclear magnetic resonance study, and relaxation dispersion measurements yield the bound fraction and time scales for the interaction of aS with CR. We find that at pH 6, CR exists as a micelle, and at a CR:aS molar ratio of ~1, only a small fraction of aS (~2%) is bound to these micelles. Rapid exchange ($k_{ex} \sim 3000$ s^{-1}) between the free and CR-bound states broadens and strongly attenuates resonances of aS by two processes: a magnetic field-dependent contribution, caused by the chemical shift difference between the two states, and a nearly field-independent contribution caused by slower tumbling of aS bound to the CR micelle. The salt dependence of the interaction suggests a predominantly electrostatic mechanism for the 60 N-terminal residues, while the weaker interaction between residues 61−100 and CR is mostly hydrophobic. Chemical shift and transferred NOE data indicate that aS becomes slightly more helical but remains largely disordered when bound to CR. Results indicate that inhibition of fibril formation does not result from binding of CR to free aS and, therefore, must result from interaction of aS fibrils or protofibrils with CR micelles.
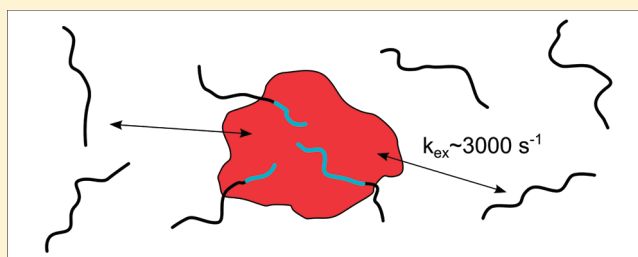
Congo Red (CR) is a histological dye that is often used to stain amyloid fibrils. While CR was long assumed to bind specifically to β-sheet structures found in amyloids, it has been demonstrated that it can in fact interact with any secondary structure, and the strength of this interaction is mostly determined by the particular side chains presented by the protein.[1] CR has been reported to inhibit certain dehydrogenases and kinases by mimicking nucleotides and coenzymes.[2] However, more recently, the fact that CR also belongs to a class of promiscuous inhibitors often picked up in high-throughput screens has become recognized. The common feature of these molecules is their propensity to self-aggregate and sequester proteins on the surface of the aggregate.[3,4] This inhibitory effect can be removed by detergents that dissolve the colloidal particles, suggesting they also act through a mechanism in which the protein binds to CR aggregates.[5] CR also has been tested for inhibition of amyloid formation and was demonstrated to be effective when used at relatively high concentrations.[6,7] However, at very low concentrations, CR can promote fibril formation in some proteins,[8] raising further questions regarding the therapeutic potential of this class of inhibitors.

Two recent NMR studies showed the presence of a relatively strong interaction between CR and monomeric aS, manifesting itself in dramatic attenuation of the NMR resonances in the N-terminal half of the protein.[9,10] Details of the mechanism underlying this broadening remained unclear, but Lendel et al.[10] concluded that binding at pH 7.4 proceeds through

formation of rapidly diffusing, small oligomeric species. These authors also proposed that binding of intrinsically unstructured proteins benefits from a large interaction surface that could compensate for the entropic cost of binding. Both studies examined the interaction between aS and CR by mapping the decrease in NMR resonance intensity observed upon binding of CR to the sequence of aS, but neither study reported on the relation between the observed resonance attenuation and the magnitude of the chemical shift change between aS in the absence and presence of CR, necessary to quantitatively evaluate the kinetics and equilibrium of the binding process. Instead, regions in the aS amino acid sequence exhibiting the largest NMR signal attenuation were interpreted as the sites directly interacting with individual CR molecules. Lendel et al. used a variety of additional biophysical techniques, including isothermal titration calorimetry, to generate binding curves for the aS−CR interaction.[10] Their data could be well fitted to a one-site model in which eight CR molecules bind with a relatively tight apparent binding constant (K_d) of 0.4 μM to aS. Although this result is compatible both with binding of aS to large CR oligomers in a 1:8 molar stoichiometry and with binding of eight individual CR molecules to a single aS protein, forming a small oligomeric unit, results of NMR-based diffusion

experiments led the authors to conclude that this latter case applies for the CR−aS interaction.[10]

There are remarkable similarities between observations made for binding of aS to CR and to phospholipids. High CR:protein ratios protect against fibril formation,[7,5,11] whereas low ratios for some proteins can induce the loss of tertiary structure and concomitant formation of fibrils or amorphous aggregates.[8,10] Analogously, high phospholipid:aS stoichiometries can protect against fibril formation, whereas low ratios can promote this process.[12−17] A second striking similarity for the interaction between aS and phospholipids versus CR relates to the impact of such binding on the intensities of NMR resonances in ^{1}H−^{15}N heteronuclear single-quantum correlation (HSQC) spectra, where intensities of the first 100 residues are greatly attenuated upon binding to either lipid vesicles or CR.[9,10,18,19]

Although at first sight the patterns of NMR intensity attenuation upon binding of aS to phospholipids and CR appear to be very similar, there is a subtle but fundamental difference, too. When interacting with CR, aS amide groups show small changes in chemical shifts and substantial resonance broadening, whereas binding to phospholipid vesicles results in resonance attenuation without concomitant shifts in the remaining peaks, and only a very slight amount of line broadening compared to that for the lipid-free protein. The attenuation of resonances in the absence of significant line broadening or shifting was attributed to slow exchange between free, dynamically disordered aS and an NMR-invisible "dark state".[19] Similar dark state behavior has been reported for a number of proteins, many but not all of them in an intrinsically disordered state, capable of fibril formation.[20−22] Considering the intriguing similarities between observations when aS interacts with small unilamellar phospholipid vesicles versus CR, but the more favorable properties of CR versus those of phospholipids (including the relatively high concentration of ~5 μM below which CR has been reported not to form aggregates[2]), we here explore a more detailed characterization of the aS−CR interaction, including the kinetics and stoichiometry of binding, the conformation of aS when bound to CR, the size of the complexes formed, and the exchange of magnetization between CR and aS. Our results, obtained at pH 6, paint a picture that is somewhat different from that gleaned from prior studies at higher pH values and indicate that under equi-stoichiometric conditions only a small fraction of aS is bound to CR, and the CR-bound form corresponds to relatively large aggregates, as confirmed by dynamic light scattering (DLS) and small-angle X-ray scattering (SAXS) measurements.

■ EXPERIMENTAL PROCEDURES

Sample Preparation. Human wild-type aS was expressed and purified as described previously.[19] Protein was produced with three labeling patterns. Perdeuterated ^{15}N-labeled protein was produced by growing bacteria in D$_2$O-based M9 medium with 1 g/L ^{15}NH$_4$Cl, 2 g/L deuterated [^{12}C]glucose, and 1 g/L ^{2}H, ^{15}N Isogro (Sigma-Aldrich, St. Louis, MO) . Triply labeled aS was produced in the same way but using deuterated [^{13}C]glucose and ^{2}H, ^{13}C, ^{15}N Isogro. The fully protonated, ^{15}N-labeled form was produced by culturing bacteria in H$_2$O-based M9 medium containing 1 g/L ^{15}NH$_4$Cl and supplemented with a MEM vitamin solution (Invitrogen).

Congo Red was purchased from Sigma-Aldrich and used without additional purification. Stock solutions of 2 and 20 mM

CR were prepared in NMR buffer [20 mM phosphate (pH 6)], with the pH readjusted to 6 if necessary. The stock solutions were unstable at room temperature, forming a thick non-transparent precipitate over time. When the NMR samples were prepared, the appropriate CR stock solution was heated and thoroughly vortexed and added to an aS solution to the desired concentration. The presence of CR precipitate particles could easily be detected from a cloudy appearance of the sample. To ensure complete dissolution, the NMR sample was warmed to 37 °C for 5 min. The resulting solution was then perfectly transparent.

NMR Spectroscopy. All experiments were performed at 15 °C in 20 mM phosphate buffer (pH 6) unless stated otherwise. To gain a more quantitative understanding of the kinetics of the binding process, we conducted relaxation dispersion experiments using a pulse sequence that measures the chemical exchange contribution for the TROSY component of the ^{15}N magnetization, thereby maximizing its fractional impact.[23] Off-resonance and pulse imperfection effects were minimized by using the four-pulse phase scheme of ref 24. CPMG experiments were performed with a fixed relaxation time but a changing number of pulses to achieve different effective fields.[25] Experiments were conducted at 500 and 900 MHz, with relaxation times of 100 and 50 ms, respectively, to compensate for the faster relaxation at 900 MHz. In each experiment, seven two-dimensional spectra were acquired in an interleaved manner, corresponding to a reference data set (no relaxation period), and spectra in which the evolution of ^{15}N was preceded by a relaxation period during which effective CPMG fields of 80, 160, 240, 400, 640, and 960 Hz were used.

Dynamic Light Scattering. DLS experiments were performed on a Malvern Zetasizer Nano instrument at 15 °C. Sample conditions were 200 μM aS and 200 μM CR in either 20 mM phosphate (pH 6) or 100 mM Tris (pH 7.4). Results were analyzed using the instrument's Malvern software.

SAXS Data Collection and Analysis. Solution X-ray scattering data were acquired at beamline 12-IDC at the Advanced Photon Source (Argonne National Laboratory, Argonne, IL). Data were collected using a mosaic Gold CCD detector positioned 3.7 m from the 1 mm diameter capillary containing the samples, using 18 keV incident radiation. The q axis was calibrated using a silver behenate sample. A total of 20 sequential data frames with 1.0 s exposure times were recorded with the samples kept at 25 °C. To prevent radiation damage, 125 μL samples were slowly pulled during data collection using a flow-through setup. Individual data frames were masked, corrected for the detector sensitivity and solid angle for each pixel, radially integrated, and normalized by the corresponding incident beam intensities. The final one-dimensional scattering profiles and their uncertainties were calculated as means and standard deviations over the 20 individual frames. The buffer data were then subtracted from the sample data. Finally, the scattering data for aS were subtracted from the data for both aS and CR using a scaling factor of 0.97. To evaluate the magnitude of a possible structure factor, data for aS and data for both aS and CR were collected at concentrations of 230, 58, 46, and 29 μM. The final subtracted data at all these concentrations proved to be indistinguishable when $q \geq 0.013$ Å^{-1}. Here, q is defined as $4\pi \sin(\theta)/\lambda$, where 2θ is the scattering angle and λ is the incident radiation wavelength.

The final subtracted data collected for 230 μM samples were fitted in the q range between 0.013 and 0.040 Å^{-1} by a function representing the sum of the scattering contributions from a

population of uniformly filled spheres of two sizes. In addition to the radii of the two spheres and the ratio of their populations, a constant offset and the buffer rescaling factor were allowed to vary, as used previously,[26] with the scattering intensity from a sphere calculated as

$$I(q) \sim V^2 \left[3 \frac{\sin(qR) - qr \cos(qR)}{q^3 R^3} \right]^2$$

where V is the volume of the sphere and R its radius.

■ RESULTS

Aggregation of Congo Red. Although there is consensus about the fact that CR can aggregate and form ribbonlike micelles, experimental studies reached rather divergent conclusions about the size of these aggregates and the critical micelle concentration (cmc). Early studies, conducted at pH 6 and 30 and 40 °C, showed that CR aggregation varies with ionic strength and temperature, with a higher temperature decreasing the extent of micelle formation and salt having the opposite effect, and suggested a cmc at 30 °C as high as 300 μM.[27] Experiments in low-salt, pH 7.5 buffer at 25 °C revealed spectroscopic signs of aggregation at a much lower CR concentration of 5 μM.[2] DLS measurements on a 2 mM CR solution (pH 8.6, 100 mM NaCl, 25 °C) suggested small size oligomers with a 1.4 nm radius,[28] whereas 2 mM CR solutions at pH 6 quickly turned opaque and yielded a precipitate. A 200 μM solution of CR in pH 6 buffer remains stable at room temperature, yet at 4 °C, some CR precipitation is observed overnight. This indicates that at lower pH values and temperatures the size of CR aggregates increases to form visually observable, light scattering complexes, with sizes on the order of hundreds of nanometers.

Remarkably, we find that a 200 μM solution of CR (pH 6) in the presence of 200 μM α-synuclein does not yield a precipitate even over a period of months at 4 °C. This supports the presence of previously described interactions between aS and CR.[9,10] Like apolipoproteins, aS contains 11-residue repeats that carry the signature of an amphipathic helix,[29] and our data suggest that aS also has detergent-like properties. However, the CR solubilizing ability of aS is found to be insufficiently strong to dissolve preformed CR precipitate in a reasonable amount of time.

NMR spectra recorded by us on CR solutions at pH 6 in 50% 2-propanol show monomeric CR behavior at 0.5 μM, but evidence of rapid exchange with an oligomeric form at a concentration as low as 2 μM (Figure S1 of the Supporting Information). In the absence of 2-propanol, the ^{1}H NMR resonances of CR remain extremely broad even at 0.5 μM, over the entire pH range of 6–8.6, indicating the cmc falls below 0.5 μM over that pH range (Figure S1 of the Supporting Information), even though the extent of formation of very large, precipitating aggregates is reduced at the higher pH.

Impact of CR on the NMR Spectrum of α-Synuclein. By using perdeuterated aS, which yields superior resolution in its heteronuclear single-quantum correlation (HSQC) NMR spectra, lacking the $^3J_{HNH\alpha}$ couplings and yielding narrower line widths, very highly resolved spectra could be obtained in the absence of CR. This allows nearly every resonance to be uniquely resolved at a spectrometer frequency of 800 MHz (Figure 1A). The high spectral resolution that can be obtained for such [^{2}H,^{15}N]aS makes it possible to follow the effect of CR
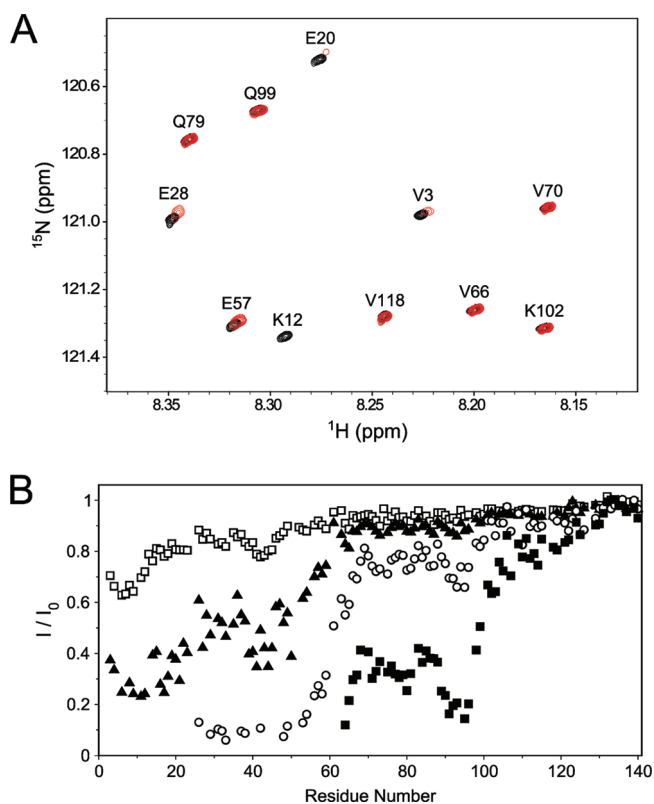

Figure 1. Impact of the presence of Congo Red on the ^{1}H–^{15}N TROSY-HSQC spectrum of aS. (A) Overlay of a small expanded region of the TROSY-HSQC spectra of the free aS sample (black) and a sample with 200 μM aS and 160 μM CR (red). Spectra were recorded at 800 MHz with a 750 ms acquisition time in each dimension. Small shifts and broadening of peaks in the presence of CR are observed for residues 1–60 (region I). (B) Ratios of aS TROSY-HSQC peak heights in the presence of different concentrations of CR compared to free aS. Spectra were recorded at a 500 MHz frequency with a 170 ms acquisition time in both dimensions and apodized with a cosine bell window function in both dimensions. The following CR:aS molar ratios are presented: 1:4 (□), 1:2 (▲), 2:1 (○), and 8:1 (■). Error bars are smaller than the symbols. At high CR concentrations, most N-terminal peaks are broadened beyond detection.

binding in great detail. Upon addition of 160 μM CR to a 200 μM aS solution, line broadening and small chemical shift changes are observed for the backbone amides of the 60 N-terminal residues. When the CR concentration is increased in a stepwise fashion, these residues are further attenuated until they fall below the detection threshold (Figure 1B). Upon dilution of an equi-stoichiometric aS/CR solution, the N-terminal residues regain intensity when the concentration is reduced to ~2 μM (Figure S2 of the Supporting Information), analogous to prior observations,[9,10] and remarkably similar to what was seen for aS in the presence of very low concentrations of small unilamellar vesicles composed of a mixture of lipids.[19]

The resonance intensity attenuation profile (Figure 1B) can be subdivided into the following regions of similar behavior: (I) N-terminal residues V3–H50, a transition region (I–II) encompassing residues G51–V63, (II) the "center" region, including residues T64–K97, and (III) the C-terminal region, residues D98–A140. The latter can be subdivided into (IIIA) D98–P120, which show some attenuation at higher CR:aS

ratios, and (IIIB) D121−A140, whose intensities remain virtually unaffected.

When the change in chemical shift as a function of residue is monitored, on average small upfield changes are observed for residues in region I, for both ^{15}N and $^{1}H^{N}$, whereas residues in C-terminal region IIIB show mostly small downfield chemical shift changes upon addition of an approximately equimolar fraction of CR to the aS sample (Figure 2). Remarkably,
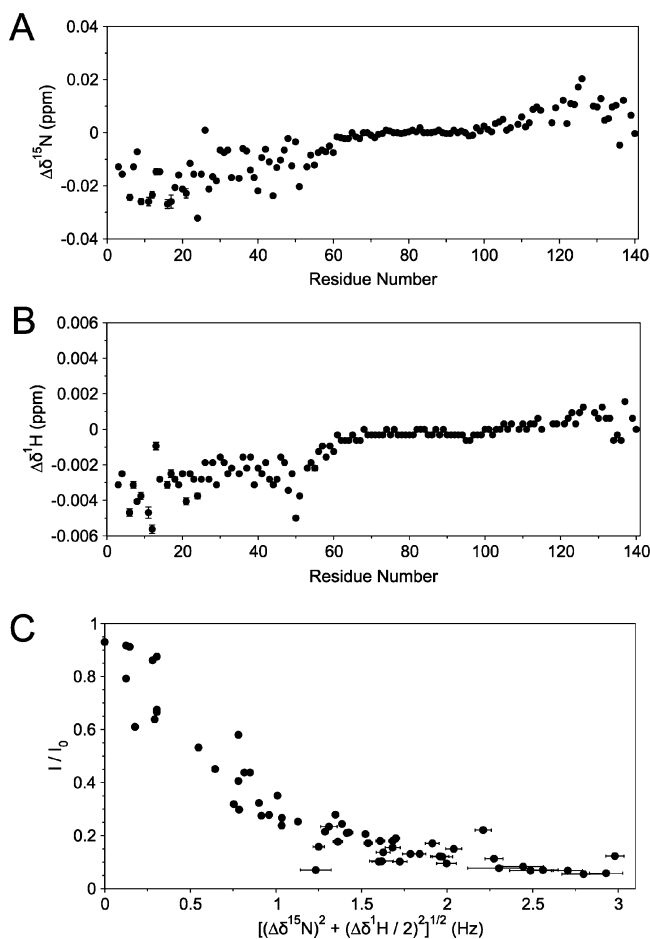
Figure 2. Chemical shift changes, $\Delta\delta$, relative to free aS induced at a 0.8:1 CR:aS ratio, as measured at a 800 MHz ^{1}H frequency and 200 μM aS. ^{15}N (A) and ^{1}H (B) chemical shift changes are shown. (C) Attenuation of peak intensities vs the weighted chemical shift change for residues 3−70, as compared to a sample of free protein. Spectra were recorded with a 750 ms acquisition time in each dimension and apodized with a 45°-shifted sine bell window function in each dimension. The ^{1}H chemical shift change is scaled by $^{1}/_{2}$ to account for the ~2-fold larger line width in the ^{1}H dimension than in the ^{15}N dimension for the free protein. Where not shown, error bars are smaller than the symbols.

resonance positions of residues in region II remain virtually unaffected by the equi-stoichiometric presence of CR, and resonance attenuation of these residues, as well as of the C-terminal residues, is minimal. A plot of the intensity attenuation caused by the addition of CR for region I versus the small frequency differences seen in the HSQC spectrum, $[(\Delta\delta^{15}N)^2 + (\Delta\delta^{1}H/2)^2]^{1/2}$, shows the attenuation is strongly correlated with the chemical shift change (Figure 2C) and therefore can be attributed to a chemical exchange process. The observation that no significant attenuation is seen for region III, despite

significant chemical shift changes, indicates that these chemical changes are not directly correlated with the exchange process observed for region I. At higher CR concentrations, where attenuation in resonance intensity becomes significant for residues in region II, changes in resonance position are observed for this region, too (Figure S3 of the Supporting Information), indicating that it also becomes involved in CR binding.

Impact of Ionic Strength on the CR−aS Interaction. The mode of interaction between CR and proteins remains the subject of considerable debate. Although there is a substantial amount of evidence of electrostatic interaction,[1,30−32] other reports suggest that specific or hydrophobic interactions are involved.[33−35] The fact that CR molecules carry two negatively charged sulfonate groups, together with the NMR observation that the positively charged N-terminal region of aS is most affected by the presence of CR, indeed suggests that the interaction of the N-terminus includes a significant electrostatic component.

Attenuation of the intensity and changes in resonance position of the backbone amide $^{1}H−^{15}N$ correlations provide site-specific probes for monitoring the impact of salt on the CR−aS interaction. A stepwise increase in ionic strength shows a pronounced impact on the attenuation profile observed in the NMR spectra (Figure 3). At 200 mM NaCl, no measurable
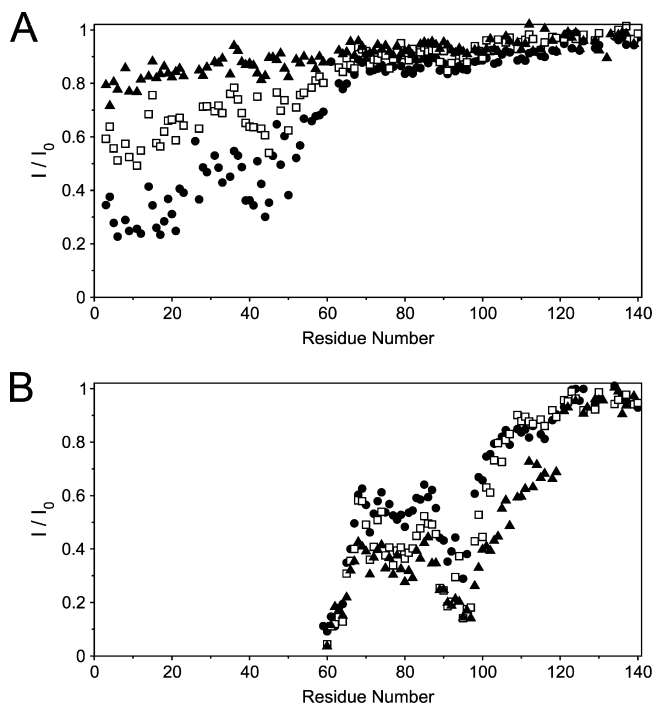
Figure 3. Attenuation of TROSY-HSQC $^{1}H−^{15}N$ correlation intensities, I/I_o, as a function of residue number for two different CR:aS stoichiometries, (A) 0.8:1 and (B) 4:1, using 200 μM aS. Attenuation ratios with respect to samples of free aS are reported for three different ionic strength conditions: standard NMR buffer (20 mM phosphate) (●), additional 100 mM NaCl (□), and additional 200 mM NaCl (▲). Spectra were recorded at a 500 MHz frequency with a 170 ms acquisition time in both dimensions and apodized with a cosine bell window function in both dimensions. Intensity uncertainties resulting from random errors are smaller than the symbols.

shifting of HSQC peak positions or significant attenuation of resonance intensities is observed anymore when small amounts of CR are added to the sample (Figure 3A), confirming the importance of the electrostatic contribution to the CR−aS interaction for region I. At a higher CR:aS ratio of 4, the N-terminal residues remain fully attenuated, even when the salt concentration is increased. Interestingly, however, region II undergoes a slight increase in its level of attenuation with increasing ionic strength (Figure 3B). This region includes the highly hydrophobic stretch of residues, V66−A78. Remarkably, at 200 mM NaCl, C-terminal segment IIIA, D98−P120, which carries numerous negatively charged residues, in addition to a substantial number of hydrophobic amino acids, is also attenuated considerably. These observations indicate that for the T64−P120 region, electrostatic repulsion between aS and CR is mitigated by the increase in ionic strength, and that the interaction is hydrophobically driven. In addition, weakening of the electrostatic interaction between the 60 N-terminal residues of aS and CR at elevated ionic strengths allows the V66−P120 region to compete more effectively with the N-terminal region for the small amount of CR surface area available per aS molecule at the low CR:aS stoichiometric ratios (0.8−4.0) used in our study.

Kinetics of CR−aS Binding. The finding that the attenuation in resonance intensity, seen in Figure 1, correlates with changes in chemical shift, $\Delta\omega$, points to a fast exchange mechanism between CR-free and CR-bound states of aS. In the limit of fast exchange, where $k_{ex} \gg \Delta\omega$, the expected line broadening contribution to R_2 for two-state exchange between states A and B is given by[36]

$$R_{ex} = p_A p_B (\Delta\omega)^2 / k_{ex} \tag{1}$$

where k_{ex} equals the sum of the forward and backward rate constants, $k_{A,B} + k_{B,A}$, and the population of site A is given by $p_A = k_{B,A}/k_{ex}$ and $p_B = 1 - p_A$. Indeed, when the transverse ^{15}N relaxation rate, R_2, for the first 60 residues is plotted versus the square of the ^{15}N chemical shift change, $(\Delta\omega)^2$, a nearly linear correlation is observed for data recorded at a 500 MHz ^1H frequency (Figure 4). Transverse relaxation rates were also measured at a 900 MHz ^1H frequency and again steeply increase with larger $\Delta\omega$ values. However, at a magnetic field that is this strong, the $k_{ex} \gg \Delta\omega$ condition is met only for residues with relatively small $\Delta\omega$ values between the free and bound states, and residues exhibiting the largest chemical shift differences, such as V16 and A17, then shift to the intermediate exchange regime (Figure 4).

In the limit where $\Delta\omega = 0$, R_2 is given by the weighted average of the transverse relaxation rates in the free (A) and bound (B) states:

$$R_2 = p_A R_{2,A} + p_B R_{2,B} \tag{2}$$

The intercept with the y axis in Figure 4 shows a value of ∼5 Hz, well above the rates, $R_{2,A}$, of ∼2 Hz, measured for the free protein (horizontal dotted line in Figure 4). This points to a significant and approximately uniform contribution from $p_B(R_{2,B} - R_{2,A})$ in eq 2, indicative of faster transverse relaxation, i.e., slower tumbling, in the CR-bound state.

To gain a more quantitative understanding of the kinetics of the binding process we conducted relaxation dispersion experiments. These experiments measure the decay of magnetization during a fixed amount of time (100 ms at 500 MHz and
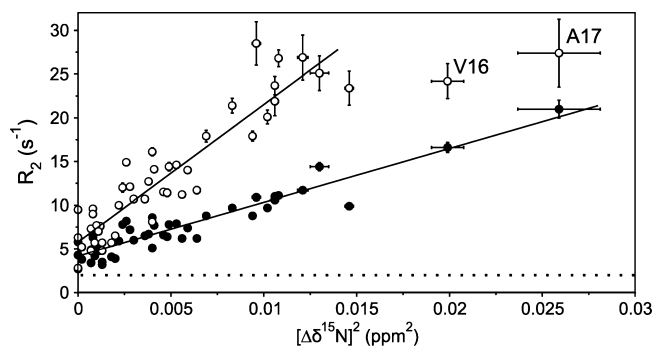

Figure 4. Plot of ^{15}N transverse relaxation rates vs the square of the ^{15}N chemical shift difference between the CR-containing sample (200 μM aS and 260 μM CR) and CR-free aS. R_2 values were measured using a Carr−Purcell−Meiboom−Gill pulse train of 180° pulses, spaced by 6.25 ms (corresponding to an 80 Hz effective field), as described by Mulder et al.[25] Measurements were taken at 500 MHz (●) and 900 MHz (○) ^1H frequencies. Solid lines represent linear fits of the data. Notice that resonances of residues V16 and A17 experience the largest chemical shift change and fall in the intermediate exchange limit at 900 MHz. The horizontal dotted line corresponds to the average R_2 for the C-terminal residues that are not involved in the interaction with CR.

50 ms at 900 MHz) as a function of the number of 180° pulses applied during this period.

Characteristic relaxation dispersion decay curves (Figure 5) for residues located in region I can be fitted with equations
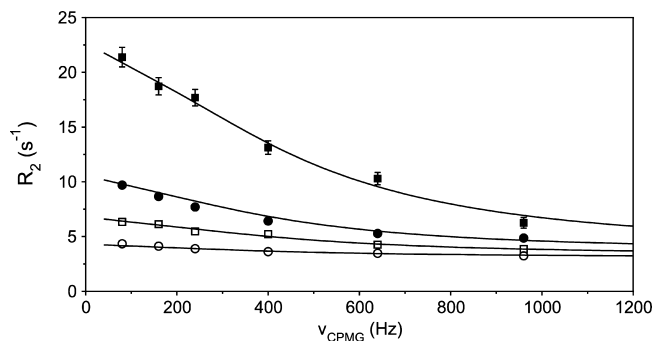

Figure 5. Characteristic relaxation dispersion curves, measured at a CR:aS ratio of 1.3:1, at 500 MHz (circles) and 900 MHz (squares). Curves are shown for E20 (filled symbols) and V26 (empty symbols).

presented by Millet et al.[37,38] and yield for each amide its k_{ex}, $\Delta\omega$, p_B, and the relaxation rate in the bound state, $R_{2,B}$. As expected for the case in which all amides in region I are part of the same binding process, k_{ex} and p_B values fitted for the individual amides that show significant relaxation dispersion cluster in a narrow range. Indeed, a more robust fit that forces all residues to be fitted with the same k_{ex} and p_B values yields the following: $k_{ex} = 2900 \pm 300$ s^{-1}, $p_B = 0.021 \pm 0.009$, and $R_{2,B}^{500\ MHz} = 111 \pm 24$ s^{-1} (close to the average values obtained in the individual fits). As these numbers indicate, only a small fraction (∼2%) of aS is bound to CR at any given time. However, the exchange kinetics are such that the region I amides have strongly attenuated intensities in the NMR HSQC spectrum.

As described above, binding of aS to CR is very tight under our buffer and temperature conditions, yet only 2% of aS is found to be bound to CR for concentrations of aS and CR of ∼200 μM. The implication, therefore, is that under these

conditions binding is saturated, and the number of "binding sites" for aS on the CR micelles can accommodate only 2% of the total protein.

At the higher CR:aS ratio of 4, region I is attenuated beyond detection, but relaxation properties of resonances for region II, which are attenuated by ~50%, yield some insights into its interaction with CR. Importantly, the difference in the ^{15}N R_2 relaxation rates measured at 500 and 800 MHz was much smaller than would be expected if the broadening were dominated by chemical exchange, in particular for residues 65−88 (Figure S4A of the Supporting Information).

Two sets of residues in region II show substantial chemical exchange contributions to their amide ^{15}N R_2 rates: 60−64 and 89−97. These residues exhibit a faster transverse relaxation rate at higher magnetic fields, as well as the largest downfield nitrogen chemical shift differences compared to free aS (Figure S4 of the Supporting Information). However, the exchange is too fast to be suppressed with a 1 kHz CPMG field. This then makes it difficult to determine the rate of the exchange process and to pin down accurately the population of the bound fraction for region II. Our finding that the R_2 rate observed for most of region II at a 4:1 CR:aS ratio is comparable to the y intercept $[\Delta\delta_{^{15}N} = 0$ (Figure 4)] of region I at a 1.3:1 CR:aS ratio suggests that the bound populations for these two cases are similar, i.e., ~2%. At the same time, the bound population for region I is expected to nearly triple at this 3-fold higher CR:aS ratio, but with the NMR intensity of the region I amides below the detection threshold, it cannot be quantified from the NMR data. Together, these considerations suggest that region II is binding as an extension to the interaction of region I, with region II binding to CR micelles for approximately one-third of the proteins that are already anchored through region I. Samples at CR:aS ratios of ≥4 are not indefinitely stable and start becoming opaque after ~24 h, indicative of the formation of larger particles. This observation indicates that at these higher stoichiometries, aS is unable to completely inhibit the formation of larger CR aggregates.

Structure of aS in the CR-Bound State from Transferred NOE. Transferred NOE (TrNOE) measurements provide a convenient site-specific method for probing the secondary structure of aS in the CR-bound state.[39,40] Previous TrNOE measurements investigating the structure of aS when bound to phospholipids yielded relatively strong sequential H^N−H^N $[d_{NN}(i,i+1)]$ NOE connectivities for the 100 N-terminal residues of the protein, with considerable spin diffusion $[d_{NN}(i,i+n); n \leq 6]$ to adjacent amide groups.[19] Because of the slow exchange kinetics observed for that system, short mixing times could not be used to eliminate indirect spin diffusion effects.[41] A second problem with quantitative interpretation of the d_{NN} connectivities on perdeuterated aS is that one cannot distinguish whether this NOE pattern, compatible with an α-helical conformation, is unique or whether the TrNOE pattern could represent only a subset of the conformations sampled by the protein in its lipid-bound state. For our study of the aS−CR interaction, the situation is more favorable, as the exchange between the free and CR-bound states is fast compared to the NOE buildup rate, permitting more quantitative analysis. Also, the ratio of sequential H^α−H^N $[d_{\alpha N}(i,i+1)]$ and intraresidue $d_{\alpha N}(i+1,i+1)$ intensities in protonated proteins provides an excellent measure of the ψ angle of residue i and can be used to probe the presence or absence of helical and extended backbone conformations.[42] Here, we use a combination of both types

of TrNOE data to probe the aS backbone when it is bound to CR. For region I, the measurements are taken at a CR:aS ratio of 1, whereas the remainder of the protein is probed at a CR:aS ratio of 4.

For β-sheet conformations, the expected sequential to intraresidue H^α−H^N distance ratio equals 0.75, versus 1.25 for the α-helix. This corresponds to expected intraresidue to sequential NOE buildup rate ratios of ~1:6 for β-sheet and 4:1 for α-helix. Although measurement of $d_{\alpha N}(i,i)/d_{\alpha N}(i−1,i)$ NOE ratios for intrinsically unstructured proteins is frustrated by poor resonance dispersion in both the H^N and H^α regions, a substantial set of such intensities could be measured by using three-dimensional (3D) ^{15}N-dispersed NOESY spectra with relatively long sampling times in all three dimensions (Figure S5 of the Supporting Information). Experimentally, we find that for regions in aS not affected by CR binding, both intraresidue and sequential NOE buildup rates are small (Figure 6A), ~0.17 ± 0.06 and ~0.7 ± 0.3 s^{-1}, respectively, yielding an average $d_{\alpha N}(i,i)/d_{\alpha N}(i−1,i)$ NOE ratio of 0.28 ± 0.11 (Figure 6B), typical for an intrinsically unstructured protein. In the presence of CR in a 1:1 molar ratio, $d_{\alpha N}(i−1,i)$ rates increase approximately 2.3-fold, whereas $d_{\alpha N}(i,i)$ NOE buildup rates for region I are ~3-fold faster, with an approximately 25% increase in their ratio compared to that of residues unaffected by CR binding (Figure 6B,C). This corresponds to a $d_{\alpha N}(i,i)/d_{\alpha N}(i−1,i)$ ratio of ≈0.4 in the CR-bound state. The finding that the TrNOE intensities, reflecting the bound state, are compatible with neither helix nor sheet conformation points to either a dynamically disordered state for aS when it is bound to the CR micelles or a static conformation in which the sequential H^α−H^N distance is slightly shorter than the intraresidue H^α−H^N distance, such as found, for example, in a polyproline helix conformation. However, the latter is inconsistent with a substantial increase in the sequential H^N−H^N NOE intensity upon CR binding (vide infra), leading us to conclude that the bound state must sample a distribution of conformations.

The relaxation dispersion measurements reported above indicate a bound fraction for region I of ~2% for the CR:aS ratio of 1.3, or ~1.6% at the CR:aS ratio of 1.0 used for the TrNOE experiments. The experimentally observed increase in $d_{\alpha N}(i,i)$ NOE buildup rate from ~0.2 to ~0.5 s^{-1} in region I therefore corresponds to an ~60-fold larger increase in NOE buildup rate for the CR-bound state, i.e., a buildup rate of ~18 s^{-1}. If the positive ϕ region, which is energetically unfavorable for most residues, is excluded, the intraresidue H^N−H^α distances span a relatively narrow range from ~2.7 to 3.0 Å. Assuming an average distance of 2.8 Å, the experimentally observed $d_{\alpha N}(i,i)$ NOE buildup rate in the bound state then corresponds to a rotational correlation time of ~180 ns.

Measurements of TrNOE on a protonated sample with a CR:aS ratio of 4 confirm that region II becomes involved in binding at these higher CR concentrations. Indeed, the NOE buildup rate of region II at a CR:aS ratio of 4 increases to values similar to those observed for region I at a CR:aS ratio of 1 (Figure 6A). A slight increase in the $d_{\alpha N}(i,i)/d_{\alpha N}(i−1,i)$ ratio is also observed for region II (Figure 6B,C) and is most pronounced for residues 89−98 (this region also showed a chemical exchange contribution to the ^{15}N transverse relaxation rates, vide supra).

A perdeuterated aS sample permitted us to record very highly resolved 3D ^{15}N−^{15}N−^{1}H NOESY spectra (Figure 7A), yielding sequential $d_{NN}(i,i+1)$ cross-peaks for the vast majority

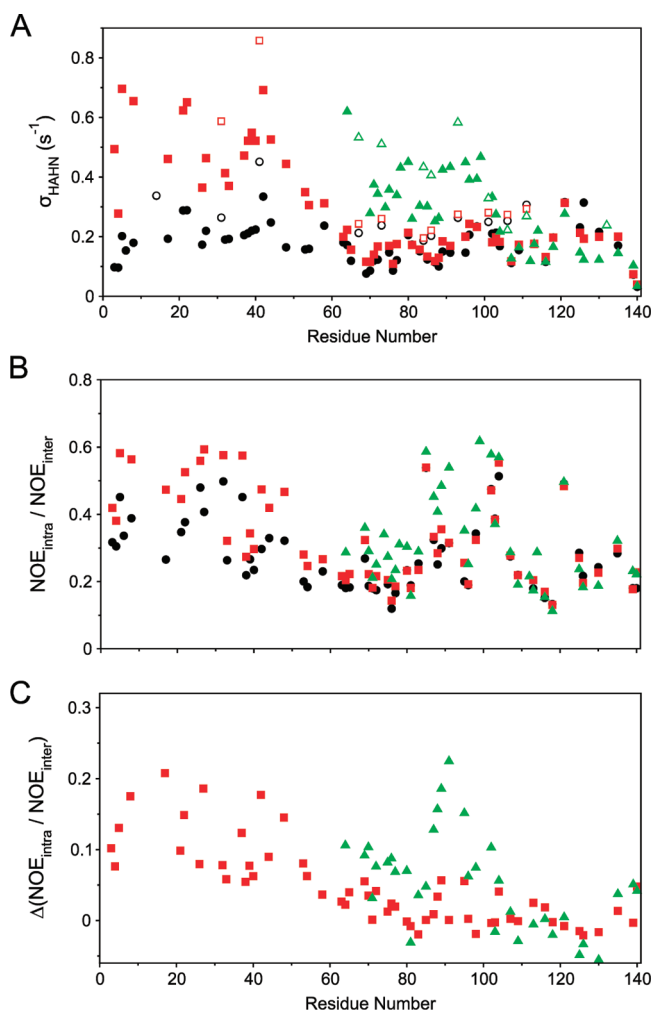**Figure 6.** Effect of Congo Red on (A) intraresidue $H^\alpha-H^N$ NOE buildup rate and (B) the ratio of intraresidue to inter-residue (from H^α of the preceding residue) $H^\alpha-H^N$ NOE (600 MHz, 200 μM aS). Data shown were collected from three samples: free aS (black circles), 1:1 CR:aS (red squares), and 4:1 CR:aS (green triangles). Gly residues are shown in panel A only (empty symbols). For Gly residues, the rates were divided by 2, to correct for the presence of two H^α atoms. (C) Change in intra- to inter-residue NOE ratios induced at CR:aS ratios of 1:1 (red squares) and 4:1 (green triangles), as compared to free aS. Increased $\sigma(H^\alpha_i-H^N_i)$ cross-relaxation rates in the presence of CR for the nearly invariant intraresidue $H^\alpha_i-H^N_i$ distance correspond to an increased $J(0)$ spectral density, i.e., slower tumbling. Increased $\sigma(H^\alpha_i-H^N_i)/\sigma(H^\alpha_{i-1}-H^N_i)$ ratios (B and C) correspond to a decreased population of extended ($\psi \approx 120°$) backbone conformations upon CR binding. Experimental uncertainties in the ratios are at most ~0.03 for attenuated residues and are listed in Table S6 of the Supporting Information.

Figure 7. NOEs between backbone amide hydrogens, as measured in a 600 MHz three-dimensional (3D) NNH NOESY-HMQC experiment (200 μM aS, 200 μM CR, and 250 ms NOE mixing time). (A) Small region of the projection of the 3D spectrum on the $^{15}N-^{15}N$ plane, with dashed lines tracking a set of sequential residues. (B) Cross-peak to diagonal peak ratios of sequential i to $i + 1$ NOEs. (C) Cross-peak to diagonal peak ratios of medium-range NOEs: i to $i + 2$ (●) and i to $i + 3$ (□).

of residues, and observable $d_{NN}(i,i+2)$ and $d_{NN}(i,i+3)$ NOE cross-peaks for a significant fraction of residues in region I (Figure 7B,C). For a CR:aS ratio of 1, regions II and III exhibit $d_{NN}(i,i+1)$ NOE cross-peak to diagonal peak intensity ratios of 0.03 ± 0.01, corresponding to buildup rates of ~0.1 s^{-1}, equal to what is seen for the free protein at 15 °C, and therefore confirming the absence of binding, despite small changes in chemical shifts relative to those of the free protein (Figure S3 of the Supporting Information). For region I, a cross-peak to diagonal peak ratio of 0.09 ± 0.03 is observed, corresponding to a sequential $d_{NN}(i,i+1)$ buildup rate of ~12 s^{-1} for the 1.6%-populated CR-bound state. This increase in the sequential H^N-
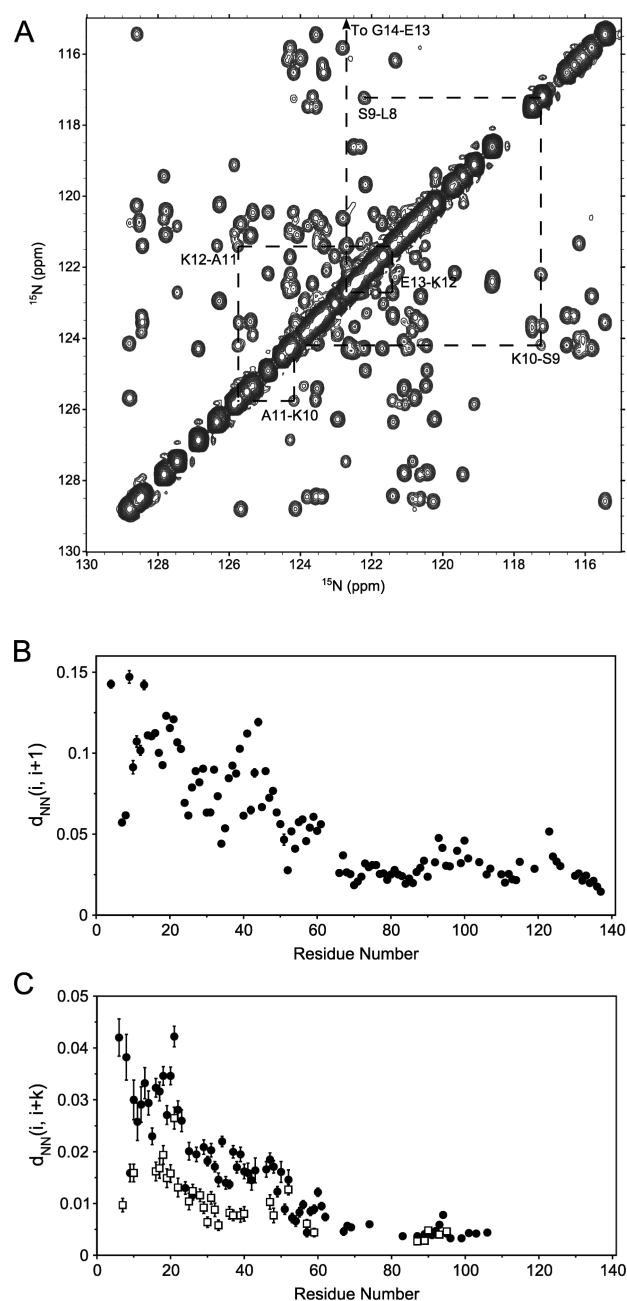
H^N cross-relaxation rate is only ~30% lower than that observed for the intraresidue H^N-H^α interaction and is equally compatible with uniform, 2.9 Å sequential H^N-H^N distances, or with a 50:50 population where this distance equals 2.7 Å in half the conformers and 3.5 Å in the other half, for example. On their own, these NOEs therefore do not allow us to determine the structure of the bound state, but the strong d_{NN} NOE connectivities in the bound state exclude the possibility of a static polyproline II helix conformation. Interestingly, residues 6−22 show somewhat higher than average $d_{NN}(i,i+1)$ NOE

buildup rates and in addition show weak $d_{NN}(i,i+2)$ and $d_{NN}(i,i+3)$ cross-peaks (Figure 7), which have intensities higher than those expected on the basis of spin diffusion, suggesting transient population of helical structure for this region of the protein. Interestingly, this region also has been implicated as the key to folding nucleation upon lipid binding.[43] On the other hand, the absence of significant $d_{\alpha N}(i,i+3)$ NOEs suggests that even this region in the CR-bound state does not adopt a pure α-helical geometry.

Secondary Structure of aS in the CR-Bound State from $^{13}C^{\alpha}$ Chemical Shifts. $^{13}C^{\alpha}$ chemical shifts are widely used as site-specific reporters for secondary structure. In α-helices, an ~3 ppm downfield chemical shift change is observed relative to random coil values, whereas extended β-sheet backbone conformations are characterized by a 1–2 ppm upfield change in chemical shift.[44,45] This change in $^{13}C^{\alpha}$ chemical shift relative to its random coil value is often termed the $^{13}C^{\alpha}$ secondary chemical shift, or $\Delta\delta^{13}C^{\alpha}$. In the absence of cosolvents or cosolutes, aS is highly disordered, and correspondingly, its $^{13}C^{\alpha}$ chemical shifts fall close to random coil values.[18] Here, we measure the change in $^{13}C^{\alpha}$ chemical shift upon addition of CR. By using the perdeuterated form of the protein, these data can be recorded with use of a 28 ms constant-time $^{13}C^{\alpha}$ evolution period, yielding 3D HNCA spectra[46] with excellent resolution in the $^{13}C^{\alpha}$ dimension and very precise $^{13}C^{\alpha}$ chemical shifts (Figure S6 of the Supporting Information). $^{13}C^{\alpha}$ chemical shift changes observed for aS upon binding to CR are found to be very small, ~0.015 ppm for residues 5–28, and even smaller for the remaining residues in region I. As expected, $^{13}C^{\alpha}$ chemical shifts do not change measurably (<0.002 ppm) for region II at the 1:1 CR:aS stoichiometry. Surprisingly, changes in region III, in particular region IIIB, are among the largest in the protein (Figure 8).
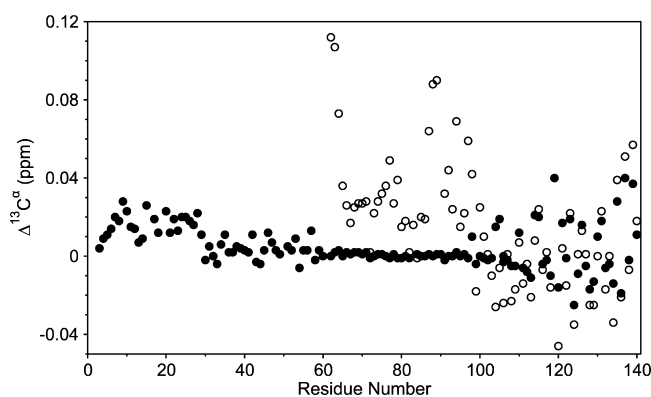

Figure 8. Changes in aS $^{13}C^{\alpha}$ chemical shifts induced by Congo Red, as measured by constant-time HNCA experiments with perdeuterated ^{13}C- and ^{15}N-labeled aS (200 μM aS, 500 MHz) for CR:aS ratios of 1:1 (●) and 4:1 (○). The experimental uncertainty is 0.002 ppm.

At the 1.3:1 CR:aS stoichiometry, our relaxation dispersion data indicate a 2.1% CR-bound fraction for the protein, corresponding to an ~1.6% bound fraction at the 1:1 CR:aS ratio used for $^{13}C^{\alpha}$ shift measurements. In the fast exchange limit, the observed $^{13}C^{\alpha}$ chemical shift is the linearly weighted average over its sampled populations, and the CR-bound $\Delta\delta^{13}C^{\alpha}$ values are ~60-fold larger than the values shown in Figure 8. However, even though the $\Delta\delta^{13}C^{\alpha}$ values are positive, indicative of an, on average, increase in the level of helical conformation, after multiplication by 60 the values remain

more than 3-fold smaller than typical α-helical $\Delta\delta^{13}C^{\alpha}$ values, even more so for residues 29–60. The very small values observed for $\Delta\delta^{13}C^{\alpha}$ strongly point to conformational averaging in the CR-bound state, with an only very modest increase in the population of α-helical backbone ϕ and ψ angles compared to what applies for disordered random coil conformations. Changes in $\Delta\delta^{13}C^{\alpha}$ for region I correlate quite well with changes in the $d_{\alpha N}(i,i)/d_{\alpha N}(i-1,i)$ ratio (Figure S7 of the Supporting Information), confirming that the $^{13}C^{\alpha}$ chemical shift changes in this region correlate with a change in the backbone ψ angles.

$\Delta\delta^{13}C^{\alpha}$ values seen for the C-terminal region III of aS are among the largest in the protein (Figure 8), but even after dividing by the fraction (~1.6%) of proteins interacting with CR micelles, we find the $\Delta\delta^{13}C^{\alpha}$ values remain small. Even though these data point to a perturbation of the average ϕ and ψ angles sampled by this segment of the protein, it clearly remains highly dynamic considering the absence of significant TrNOE effects noted above (Figure 7).

When the CR:aS molar ratio is increased to 4, many of the NMR characteristics of region II become similar to those of region I at a CR:aS ratio of 1, including the intraresidue $^{1}H^{N}-^{1}H^{\alpha}$ buildup rates noted above (Figure 6A), the ^{15}N R_2 rate (extrapolated to zero exchange contribution), and the increase in TrNOE rate, as well as the magnetization transfer from CR to aS, as probed by the Water-LOGSY experiment (vide infra). This therefore suggests a CR-bound fraction of ~2% for region II at a CR:aS ratio of 4. We observe $\Delta\delta^{13}C^{\alpha}$ values of ~0.025 ppm for most of the NAC region (residues 61–95) of the protein under these conditions, but values as high as 0.09 ppm for residues I88 and A89 (Figure 8). If these $\Delta\delta^{13}C^{\alpha}$ secondary shifts are entirely attributed to the 2% bound state, secondary shifts in the CR-bound state are ~50-fold larger and therefore indicative of a high population of α-helical backbone ϕ and ψ angles, even while not rigidly anchored to the CR micelle. I88 and A89 also show the strongest increase in $d_{\alpha N}(i+1,i+1)/d_{\alpha N}(i,i+1)$ ratio upon CR binding in the entire protein (Figure 6C).

NOE Transfer from CR Micelles to aS by Water-LOGSY. The CR micelle–aS assembly tumbles slowly in an isotropic solution. Considerable intermolecular magnetization transfer therefore is expected for proximate protons. Probing of such magnetization transfer is complicated by the very broad ^{1}H line shape of the CR (Figure S1 of the Supporting Information), whose aromatic resonances overlap with the aS backbone H^{N} resonances. This spectral property makes it difficult to probe intermolecular contacts by standard saturation transfer difference (STD) NMR experiments.[47] However, a convenient alternative way to saturate the CR resonance takes advantage of the fast hydrogen exchange of its two amino groups. Saturation of the water resonance with a weak radiofrequency field (γB_1 = 13 Hz) does not directly affect the aS amide resonances but saturates all CR ^{1}H nuclei by efficient spin diffusion from its saturated, rapidly exchanging amine groups. Magnetization exchange between CR and the backbone amide protons of perdeuterated, amide-protonated aS then manifests itself as attenuation of the amide $^{1}H-^{15}N$ HSQC intensities. This experiment is effectively equivalent to the Water-LOGSY experiment,[48,49] widely used to probe intermolecular interactions between large proteins and weakly binding ligands, but in this case, aS takes the position of the ligand and the CR micelle functions like the macromolecule in the regular Water-LOGSY experiment.

Because direct hydrogen exchange of the backbone amide protons with solvent cannot be fully eliminated by lowering the sample pH to 6.0 and lowering the temperature to 5 °C, we monitor the ratio of the attenuation factors caused by water saturation in aS samples without CR and equivalent samples containing CR in a 1:1 or 4:1 stoichiometry (Figure 9). For the
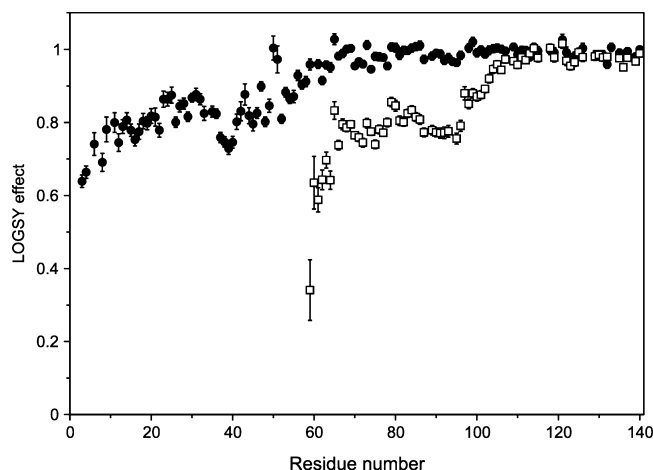

Figure 9. Water-LOGSY effect for 1:1 (●) and 4:1 (□) CR−aS samples. Experiments were performed on perdeuterated ^{15}N-labeled aS at 5 °C (pH 6.0, 200 μM aS, 500 MHz) and involved application of a 2 s presaturation pulse on water with a strength γB_1 of 13 Hz (or 0 Hz, in the no-presaturation reference experiment) followed by a normal HSQC sequence. Reference and attenuated spectra were recorded in an interleaved manner, using a room-temperature probehead. The attenuation ratio I/I_o in the presence and absence of water presaturation is measured in the presence of CR, $(I/I_o)^{CR}$, and in the absence of CR, $(I/I_o)^{free}$. The LOGSY effect plotted in the figure represents $(I/I_o)^{CR}/(I/I_o)^{free}$, thereby eliminating to first order the effect of amide hydrogen exchange with solvent at pH 6 and 5 °C.

1:1 stoichiometry, ~20% attenuation of the amide signals is observed in region I, with only very weak (<5%) attenuation in region II, and no detectable transfer for region III, confirming the nearly complete absence of direct contacts between region II and the CR micelle and the complete absence of contacts between the micelle and region III. The attenuation pattern in region I is relatively flat. In part, this may be a consequence of the very long effective NOE mixing time inherent to the Water-LOGSY experiment, which can result in extensive spin diffusion, thereby smoothing the magnetization transfer profile. However, the absence of significant variation is also compatible with a heterogeneous disordered mode of binding of aS to the CR aggregate.

When the CR:aS ratio is increased to 4:1, the Water-LOGSY experiment shows quite strong, ~25% attenuation for region II. The uniformity in the magnetization transfer from CR to the region II amide protons again points to a dynamic, heterogeneous mode of binding.

Dynamic Light Scattering and SAXS Evaluation of CR−aS Interaction. Dynamic light scattering (DLS) provides a simple and straightforward method for estimating the hydrodynamic size of the CR−aS aggregates. Analysis of the size distribution for a heterogeneous ensemble of objects can be challenging, however, with the larger objects typically being overemphasized in histograms derived from such data. With this caveat in mind, the hydrodynamic radius observed by DLS at pH 6.0 is approximately 180 Å (Figure S8 of the Supporting

Information). However, at a slightly higher pH (7.4), DLS indicates a much smaller size for CR micelles, on the order of a 15 Å radius, similar to values observed by Lendel et al.[10] This radius falls close to the value observed for the free protein and indicates that under these conditions light scattering is no longer dominated by the presence of large aggregates.

Small-angle X-ray scattering (SAXS) provides another effective tool for probing the size and shape of the CR−aS aggregates. Free aS, at the dilute concentration probed, gives a very weak scattering pattern, compatible with coil-like behavior, as shown previously.[50] In contrast, for the 1:1 aS−CR sample, strong scattering intensity is observed. However, the Guinier plot of the scattering curve, commonly used for extracting the radius of gyration, R_g, is quite nonlinear, indicative of a heterogeneous population of the aggregates. Although a size distribution cannot be derived uniquely from such a scattering profile, an estimate can be obtained by fitting the low-q region ($q = 0.013−0.04$) as that of the sum of two types of spherical objects with radii of 180 and 103 Å, and populations of 28 and 72%, respectively (Figure 10).
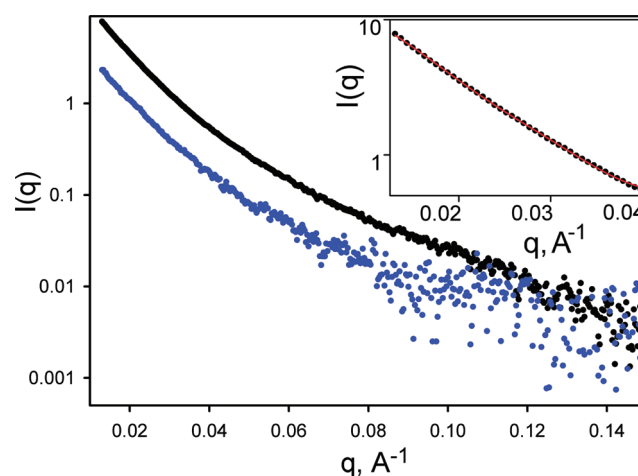

Figure 10. Small-angle X-ray scattering profiles obtained for equimolar mixtures of aS and CR at 230 μM (black dots) and 56 μM (blue dots). The inset shows the Guinier region, fitted to a profile computed for a 72% population of 103 Å radius spheres and a 28% population of 180 Å spheres (red line).

■ DISCUSSION

Our NMR data clearly indicate that CR in aqueous solution forms micelles with a cmc well below 1 μM. However, the size of the micelles is strongly pH dependent and rapidly increases below neutral pH. α-Synuclein strongly binds to these colloidal aggregates and helps prevent precipitation of CR. Although the affinity of aS for CR is quite high, the binding surface for aS on the CR aggregates is small and limited to approximately one aS molecule per 60 CR molecules. The first 60 residues of aS, which carry a net positive charge, bind the CR micelles with highest affinity, and only at a CR:aS molar ratio well above 1 do we observe evidence of additional binding of the neutral, more hydrophobic region of aS, encompassing residues 64−98. Binding of the N-terminal region to CR is strongly attenuated with increasing salt concentrations, whereas a small increase in the level of binding of the hydrophobic region is observed with increasing ionic strength.

The origin of small chemical shift changes, such as observed here for aS upon binding to CR micelles, cannot be deduced unambiguously from such data. Chemical shifts are impacted primarily by very local effects such as backbone torsion angles, steric clashes, and electric fields. The chemical shift changes for the N-terminal residues correlate with binding to the CR micelles, as evidenced by the relaxation dispersion measurements. If these chemical shift changes were to result from a change in α-helical secondary structure in the bound state, they would have to be more uniform and considerably larger than what we observe. Instead, together with NOE buildup rates and ^{15}N transverse relaxation rates, these chemical shift data point to a considerable degree of dynamic disorder in the micelle-bound state.

Our NMR data do not provide conclusive information about the nature of the interaction between aS and CR micelles. The Water-LOGSY data indicate there is considerable intermolecular magnetization transfer, which is remarkably uniform across region I, and across region II at a higher CR:aS stoichiometry. However, this experiment does not uniquely distinguish between the case in which aS engages in a dynamic interaction with the surface of CR micelles or dynamically traverses the ribbonlike micelles. Both modes appear to be compatible with the observed ability of aS to inhibit formation and precipitation of large CR micelles. However, at near neutral pH the negatively charged sulfonate moieties of CR aggregates may result in a binding surface somewhat similar to that of SDS micelles, where aS is known to bind in a surface mode.[51]

Even though the C-terminal region of aS shows small chemical shift changes upon interaction with CR, there is no direct magnetization transfer between CR and aS, as probed with the Water-LOGSY experiment. Also, the absence of increased intramolecular NOE buildup rates for the C-terminal tail residues in the presence of CR suggests that the chemical shift changes simply reflect a small difference in their conformational distribution relative to the free protein. Such a difference in conformational distribution upon CR binding is not surprising considering that weak, nonspecific, long-range electrostatic interactions between the oppositely charged N- and C-terminal regions can be seen in the free protein.[52]

Intraresidue H^N–H^α NOE buildup rates for region I in the CR micelle-bound state are ~18 s^{-1}, roughly what would be expected for a protein rigidly bound to a particle with a 100 Å diameter undergoing Brownian diffusion. However, both our DLS and SAXS data indicate that the aS–CR aggregates have diameters in the 200–400 Å range. Correspondingly, one would expect H^N–H^α NOE buildup rates much faster than 18 s^{-1} if the aS–CR aggregate were to behave like a rigid object. Instead, the slower than expected NOE buildup rates therefore point to a highly dynamic and heterogeneous mode of interaction between aS and CR, where aS retains a high degree of motional freedom. Although very small upfield changes in $^{13}C^\alpha$ chemical shifts are indicative of a shift toward α-helical conformations in the bound form, both for the N-terminal region and for the hydrophobic NAC region at higher CR:aS ratios, the magnitude of the chemical shift changes is much smaller than what would be expected for a purely α-helical bound conformation. Moreover, the ratios of intraresidue to sequential H^N–H^α NOE intensities point to a structure in the bound state that is neither extended nor α-helical, which is again indicative of a dynamically heterogeneous mode of binding.

CONCLUDING REMARKS

Inhibition of aS fibril formation by CR is quite effective when both the protein and CR are at concentrations of 100 μM,[10] but our data indicate that only a small aS fraction (<2%) interacts with CR under such conditions, i.e., that >98% of aS remains free of any interaction with CR. This result indicates that the mechanism of inhibition of fibril formation by CR must relate to interaction of CR with the fibril or its protofibril intermediate, and not to interaction with the free protein.

Although we find that the interaction between monomeric aS and CR micelles is not the mechanism by which fibril formation is inhibited, the impact on the aS NMR spectrum caused by binding of aS to CR is of interest, because at first sight it shows close similarities to the effect of interaction of aS with small amounts of phospholipid vesicles. Under such conditions, i.e., at molar concentrations of phospholipids comparable to the aS concentration, where the amount of phospholipid vesicle surface is insufficient to simultaneously bind more than only a small fraction of aS, a clear stepwise attenuation of HSQC resonance intensity as a function of residue number is observed.[19] The reason for this behavior, attributed to a NMR dark state, remains not fully understood. NMR spectra previously reported for binding of aS to CR[9,10] showed a very similar attenuation profile, and CR therefore provided an interesting alternative for further probing the interaction of aS with a lipophilic surface under conditions where there is insufficient surface area available to accommodate binding of all protein.

Although at first sight the behavior of aS upon binding to CR appears very similar to that seen for binding of the protein to very low concentrations of phospholipids, a key difference is seen in the kinetics of the process. For CR binding, a strong correlation among the chemical shift change, the degree of resonance broadening, and the attenuation of intensity is observed (Figures 2 and 4), which is the typical scenario for a system subject to fast or intermediate chemical exchange. For lipid binding, we found that the attenuation in intensity is not caused by ^{1}H or ^{15}N broadening.[19] In fact, the resonances of aS remain sharp in the presence of small amounts of lipids but simply decrease in intensity in a progressive manner toward the N-terminus of the protein. This latter behavior is expected for a system in slow exchange, on a time scale of ≥100 ms, between a random coil-like, dynamically disordered conformation and a dark state, in which resonances are severely broadened. For the interaction between aS and CR, the dichotomy between the SAXS and DLS results on one hand and H^α–H^N NOE buildup rates on the other points to a dynamically heterogeneous binding mode. It is conceivable that a similar situation applies for the dark state of aS when it interacts with very low concentrations of phospholipids, but remarkably, the rate of exchange between lipid-free aS and lipid-bound aS must remain slow for the protein to retain its narrow line widths.

ASSOCIATED CONTENT

S Supporting Information

One-dimensional ^{1}H NMR spectra of CR under different conditions, plots of peak intensity attenuation as a function of aS concentration at a CR:aS ratio of 1, TROSY spectra of free aS and a sample with a CR:aS ratio of 4, plots of ^{1}H and ^{15}N chemical shift changes induced at a CR:aS ratio of 4, plots of CPMG relaxation rates measured at 500 and 800 MHz, strip plots of the 3D HHN NOESY-HMQC spectrum measured for

a CR:aS ratio of 1, overlay of strip plots corresponding to 3D CT-HNCA spectra measured for a CR:aS ratio of 1 and free aS, plots of the change in the $^{13}C^{\alpha}$ chemical shift of residue i versus the change in $d_{\alpha N}(i+1,i+1)/d_{\alpha N}(i,i+1)$ NOE ratio, plots of DLS results for samples with a CR:aS ratio of 1 at pH 6 and 7.4, results of CPMG-based relaxation dispersion experiments conducted at 500 and 900 MHz, and tables of experimental data used for generating the figures. This material is available free of charge via the Internet at http://pubs.acs.org.

■ AUTHOR INFORMATION

Corresponding Author

*National Institute of Diabetes and Digestive and Kidney Diseases, National Institutes of Health, 5 Memorial Dr., Bethesda, MD 20892-0520. E-mail: bax@nih.gov.

■ ACKNOWLEDGMENTS

■ ABBREVIATIONS

aS, α-synuclein; NAC, non-amyloid component; cmc, critical micelle concentration; CPMG, Carr−Purcell−Meiboom−Gill; CR, Congo Red; DLS, dynamic light scattering; SAXS, small-angle X-ray scattering; HSQC, heteronuclear single-quantum correlation; TROSY, transverse relaxation-optimized spectroscopy; NOE, nuclear Overhauser effect; NMR, nuclear magnetic resonance.

■ REFERENCES

(1) Khurana, R., Uversky, V. N., Nielsen, L., and Fink, A. L. (2001) Is Congo red an amyloid-specific dye? *J. Biol. Chem. 276*, 22715−22721.
(2) Edwards, R. A., and Woody, R. W. (1979) Spectroscopic studies of cibacron blue and congo red bound to dehydrogenases and kinases: Evaluation of dyes as probes of the dinucleotide fold. *Biochemistry 18*, 5197−5204.
(3) McGovern, S. L., Helfand, B. T., Feng, B., and Shoichet, B. K. (2003) A specific mechanism of nonspecific inhibition. *J. Med. Chem. 46*, 4265−4272.
(4) McGovern, S. L., Caselli, E., Grigorieff, N., and Shoichet, B. K. (2002) A common mechanism underlying promiscuous inhibitors from virtual and high-throughput screening. *J. Med. Chem. 45*, 1712−1722.
(5) Findeis, M. A. (2000) Approaches to discovery and characterization of inhibitors of amyloid β-peptide polymerization. *Biochim. Biophys. Acta 1502*, 76−84.
(6) Feng, B. Y., Toyama, B. H., Wille, H., Colby, D. W., Collins, S. R., May, B. C. H., Prusiner, S. B., Weissman, J., and Shoichet, B. K. (2008) Small-molecule aggregates inhibit amyloid polymerization. *Nat. Chem. Biol. 4*, 197−199.

(7) Rudyk, H., Vasiljevic, S., Hennion, R. M., Birkett, C. R., Hope, J., and Gilbert, I. H. (2000) Screening Congo Red and its analogues for their ability to prevent the formation of PrP-res in scrapie-infected cells. *J. Gen. Virol. 81*, 1155−1164.
(8) Kim, Y. S., Randolph, T. W., Manning, M. C., Stevens, F. J., and Carpenter, J. F. (2003) Congo red populates partially unfolded states of an amyloidogenic protein to enhance aggregation and amyloid fibril formation. *J. Biol. Chem. 278*, 10842−10850.
(9) Rao, J. N., Dua, V., and Ulmer, T. S. (2008) Characterization of α-synuclein interactions with selected aggregation-inhibiting small molecules. *Biochemistry 47*, 4651−4656.
(10) Lendel, C., Bertoncini, C. W., Cremades, N., Waudby, C. A., Vendruscolo, M., Dobson, C. M., Schenk, D., Christodoulou, J., and Toth, G. (2009) On the Mechanism of Nonspecific Inhibitors of Protein Aggregation: Dissecting the Interactions of α-Synuclein with Congo Red and Lacmoid. *Biochemistry 48*, 8322−8334.
(11) Masuda, M., Suzuki, N., Taniguchi, S., Oikawa, T., Nonaka, T., Iwatsubo, T., Hisanaga, S., Goedert, M., and Hasegawa, M. (2006) Small molecule inhibitors of α-synuclein filament assembly. *Biochemistry 45*, 6085−6094.
(12) Perrin, R. J., Woods, W. S., Clayton, D. F., and George, J. M. (2001) Exposure to long chain polyunsaturated fatty acids triggers rapid multimerization of synucleins. *J. Biol. Chem. 276*, 41958−41962.
(13) Zhu, M., and Fink, A. L. (2003) Lipid binding inhibits α-synuclein fibril formation. *J. Biol. Chem. 278*, 16873−16877.
(14) Zhu, M., Li, J., and Fink, A. L. (2003) The association of α-synuclein with membranes affects bilayer structure, stability, and fibril formation. *J. Biol. Chem. 278*, 40186−40197.
(15) Necula, M., Chirita, C. N., and Kuret, J. (2003) Rapid anionic micelle-mediated α-synuclein fibrillization in vitro. *J. Biol. Chem. 278*, 46674−46680.
(16) Welch, K., and Yuan, J. Y. (2003) α-Synuclein oligomerization: A role for lipids? *Trends Neurosci. 26*, 517−519.
(17) Jo, E., Darabie, A. A., Han, K., Tandon, A., Fraser, P. E., and McLaurin, J. (2004) α-Synuclein-synaptosomal membrane interactions: Implications for fibrillogenesis. *Eur. J. Biochem. 271*, 3180−3189.
(18) Eliezer, D., Kutluay, E., Bussell, R., and Browne, G. (2001) Conformational properties of α-synuclein in its free and lipid-associated states. *J. Mol. Biol. 307*, 1061−1073.
(19) Bodner, C. R., Dobson, C. M., and Bax, A. (2009) Multiple Tight Phospholipid-Binding Modes of α-Synuclein Revealed by Solution NMR Spectroscopy. *J. Mol. Biol. 390*, 775−790.
(20) Zhang, X. C., Perugini, M. A., Yao, S., Adda, C. G., Murphy, V. J., Low, A., Anders, R. F., and Norton, R. S. (2008) Solution conformation, backbone dynamics and lipid interactions of the intrinsically unstructured malaria surface protein MSP2. *J. Mol. Biol. 379*, 105−121.
(21) Park, S. J., Borin, B. N., Martinez-Yamout, M. A., and Dyson, H. J. (2011) The client protein p53 adopts a molten globule-like state in the presence of Hsp90. *Nat. Struct. Mol. Biol. 18*, 537−541.
(22) Fawzi, N. L., Ying, J. F., Torchia, D. A., and Clore, G. M. (2011) Kinetics of Amyloid β Monomer-to-Oligomer Exchange by NMR Relaxation. *J. Am. Chem. Soc. 132*, 9948−9951.
(23) Loria, J. P., Rance, M., and Palmer, A. G. (1999) A TROSY CPMG sequence for characterizing chemical exchange in large proteins. *J. Biomol. NMR 15*, 151−155.
(24) Yip, G. N. B., and Zuiderweg, E. R. P. (2004) A phase cycle scheme that significantly suppresses offset-dependent artifacts in the R-2-CPMG N-15 relaxation experiment. *J. Magn. Reson. 171*, 25−36.
(25) Mulder, F. A. A., Skrynnikov, N. R., Hon, B., Dahlquist, F. W., and Kay, L. E. (2001) Measurement of slow (μs−ms) time scale dynamics in protein side chains by N-15 relaxation dispersion NMR spectroscopy: Application to Asn and Gln residues in a cavity mutant of T4 lysozyme. *J. Am. Chem. Soc. 123*, 967−975.
(26) Grishaev, A., Guo, L. A., Irving, T., and Bax, A. (2010) Improved Fitting of Solution X-ray Scattering Data to Macromolecular Structures and Structural Ensembles by Explicit Water Modeling. *J. Am. Chem. Soc. 132*, 15484−15486.

(27) Sivaraja-Iyer, S. R., and Singh, G. S. (1970) Studies on Aggregation of Dyes in Aqueous Solutions. *Kolloid Z. Z. Polym. 242*, 1196.

(28) Stopa, B., Piekarska, B., Konieczny, L., Rybarska, J., Spolnik, P., Zemanek, G., Roterman, I., and Krol, M. (2003) The structure and protein binding of amyloid-specific dye reagents. *Acta Biochim. Pol. 50*, 1213–1227.

(29) Davidson, W. S., Jonas, A., Clayton, D. F., and George, J. M. (1998) Stabilization of α-synuclein secondary structure upon binding to synthetic membranes. *J. Biol. Chem. 273*, 9443–9449.

(30) Caughey, B., Brown, K., Raymond, G. J., Katzenstein, G. E., and Thresher, W. (1994) Binding of the Protease-Sensitive Form of Prion Protein PRP to Sulfated Glycosaminoglycan and Congo Red. *J. Virol. 68*, 2135–2141.

(31) Heegaard, N. H. H., Sen, J. W., and Nissen, M. H. (2000) Congophilicity (Congo red affinity) of different β₂-microglobulin conformations characterized by dye affinity capillary electrophoresis. *J. Chromatogr., A 894*, 319–327.

(32) Inouye, H., Nguyen, J. T., Fraser, P. E., Shinchuk, L. M., Packard, A. B., and Kirschner, D. A. (2000) Histidine residues underlie Congo red binding to Aβ analogs. *Amyloid 7*, 179–188.

(33) Demaimay, R., Harper, J., Gordon, H., Weaver, D., Chesebro, B., and Caughey, B. (1998) Structural aspects of Congo red as an inhibitor of protease-resistant prion protein formation. *J. Neurochem. 71*, 2534–2541.

(34) Turnell, W. G., and Finch, J. T. (1992) Binding of the dye congo red to the amyloid protein pig insulin reveals a novel homology amongst amyloid-forming peptide sequences. *J. Mol. Biol. 227*, 1205–1223.

(35) Ashburn, T. T., Han, H., McGuinness, B. F., and Lansbury, P. T. (1996) Amyloid probes based on Congo Red distinguish between fibrils comprising different peptides. *Chem. Biol. 3*, 351–358.

(36) Grey, M. J., Wang, C. Y., and Palmer, A. G. (2003) Disulfide bond isomerization in basic pancreatic trypsin inhibitor: Multisite chemical exchange quantified by CPMG relaxation dispersion and chemical shift modeling. *J. Am. Chem. Soc. 125*, 14324–14335.

(37) Davis, D. G., Perlman, M. E., and London, R. E. (1994) Direct measurements of the dissociation-rate constant for inhibitor-enzyme complexes via the T₁ᵣ and T₂ (CPMG) methods. *J. Magn. Reson., Ser. B 104*, 266–275.

(38) Millet, O., Loria, J. P., Kroenke, C. D., Pons, M., and Palmer, A. G. (2000) The static magnetic field dependence of chemical exchange linebroadening defines the NMR chemical shift time scale. *J. Am. Chem. Soc. 122*, 2867–2877.

(39) Clore, G. M., and Gronenborn, A. M. (1983) Theory of the time dependent transferred nuclear Overhauser effect: Applications to structural analysis of ligand-protein complexes in solution. *J. Magn. Reson. 53*, 423–442.

(40) Ni, F. (1994) Recent developments in transferred NOE methods. *Prog. Nucl. Magn. Reson. Spectrosc. 26*, 517–606.

(41) Arepalli, S. R., Glaudemans, C. P. J., Daves, G. D., Kovac, P., and Bax, A. (1995) Idenitfication of protein-mediated indirect NOE effects in a disaccharide-FAB complex by transferred ROESY. *J. Magn. Reson., Ser. B 106*, 195–198.

(42) Gagne, S. M., Tsuda, S., Li, M. X., Chandra, M., Smillie, L. B., and Sykes, B. D. (1994) Quantification of the calcium-induced secondary structural changes in the regulatory domain of troponin-C. *Protein Sci. 3*, 1961–1974.

(43) Bartels, T., Ahlstrom, L. S., Leftin, A., Kamp, F., Haass, C., Brown, M. F., and Beyer, K. (2010) The N-Terminus of the Intrinsically Disordered Protein α-Synuclein Triggers Membrane Binding and Helix Folding. *Biophys. J. 99*, 2116–2124.

(44) Wishart, D. S., Sykes, B. D., and Richards, F. M. (1991) Relationship between nuclear magnetic resonance chemical shift and protein secondary structure. *J. Mol. Biol. 222*, 311–333.

(45) Spera, S., and Bax, A. (1991) Empirical correlation between protein backbone conformation and Cα and Cβ ¹³C nuclear magnetic resonance chemical shifts. *J. Am. Chem. Soc. 113*, 5490–5492.

(46) Kay, L. E., Ikura, M., Tschudin, R., and Bax, A. (1990) Three-dimensional triple-resonance NMR spectroscopy of isotopically enriched proteins. *J. Magn. Reson. 89*, 496–514.

(47) Mayer, M., and Meyer, B. (1999) Characterization of ligand binding by saturation transfer difference NMR spectroscopy. *Angew. Chem., Int. Ed. 38*, 1784–1788.

(48) Dalvit, C., Pevarello, P., Tato, M., Veronesi, M., Vulpetti, A., and Sundstrom, M. (2000) Identification of compounds with binding affinity to proteins via magnetization transfer from bulk water. *J. Biomol. NMR 18*, 65–68.

(49) Dalvit, C., Fogliatto, G., Stewart, A., Veronesi, M., and Stockman, B. (2001) WaterLOGSY as a method for primary NMR screening: Practical aspects and range of applicability. *J. Biomol. NMR 21*, 349–359.

(50) Bernado, P., Mylonas, E., Petoukhov, M. V., Blackledge, M., and Svergun, D. I. (2007) Structural characterization of flexible proteins using small-angle X-ray scattering. *J. Am. Chem. Soc. 129*, 5656–5664.

(51) Ulmer, T. S., Bax, A., Cole, N. B., and Nussbaum, R. L. (2005) Structure and dynamics of micelle-bound human α-synuclein. *J. Biol. Chem. 280*, 9595–9603.

(52) Bertoncini, C. W., Jung, Y. S., Fernandez, C. O., Hoyer, W., Griesinger, C., Jovin, T. M., and Zweckstetter, M. (2005) Release of long-range tertiary interactions potentiates aggregation of natively unstructured α-synuclein. *Proc. Natl. Acad. Sci. U.S.A. 102*, 1430–1435.